IAC-16-A3.3A.6

SMALL MARS SATELLITE: A LOW-COST SYSTEM FOR MARS EXPLORATION

Pasolini P.*[a], Aurigemma R.[b], Causa F.[a], Cimminiello N.[b], de la Torre Sangrà D.[c], Dell'Aversana P.[d], Esposito F.[e], Fantino E.[c], Gramiccia L.[f], Grassi M.[a], Lanzante G.[a], Molfese C.[e], Punzo F.[d], Roma I.[g], Savino R.[a], Zuppardi G.[a]

[a] *University of Naples "Federico II", Naples (Italy)*
[b] *Eurosoft srl, Naples (Italy)*
[c] *Space Studies Institute of Catalonia (IEEC), Barcelona (Spain)*
[d] *ALI S.c.a.r.l., Naples (Italy)*
[e] *INAF - Astronomical Observatory of Capodimonte, Naples (Italy)*
[f] *SRS E.D., Naples (Italy)*
[g] *ESA European Space Agency, Nordwijk (The Netherlands)*

* Corresponding Author

Abstract

The Small Mars Satellite (SMS) is a low-cost mission to Mars, currently under feasibility study funded by the European Space Agency (ESA). The mission, whose estimated cost is within 120 MEuro, aims at delivering a small Lander to Mars using an innovative deployable (umbrella-like) heat shield concept, known as IRENE (Italian ReEntry NacellE), developed and patented by ALI S.c.a.r.l., which is also the project's prime contractor. The Lander includes two small payloads, i.e., a dust particle analyzer and an aerial drone. The former is based on an instrument, developed by the Astronomical Observatory of Capodimonte (INAF-OAC), performing in-situ measurements of the size distribution and abundance of dust particles suspended in the Martian atmosphere. The drone is being designed by the University of Naples and aims at demonstrating the feasibility of low-altitude flight in the Martian atmosphere. The project also involves the Space Studies Institute of Catalonia (IEEC), responsible for launch and trajectory design. In the paper, we illustrate the results of the feasibility study of SMS, including a description of the mission profile, launch and escape phases, interplanetary trajectory, Mars approach, entry, descent and landing (EDL), and payload deployment and operations. The current baseline envisages launching to LEO with VEGA. Then, a dedicated propulsion module will provide a series of apogee raising maneuvers to place the vehicle on the hyperbolic trajectory to Mars. A targeting maneuver, provided by a cruise stage, will direct the spacecraft to the atmospheric entry point providing initial conditions suitable for the deployment of the heat shield. This will provide a ballistic coefficient much lower than in previous Mars missions, thus allowing to reach subsonic conditions without the use of a supersonic parachute. To demonstrate this, EDL and aero-thermo-dynamic analyses are performed with a 3-DoF model of the entry trajectory and high fidelity CFD and DSMC analysis tools. Finally, particular attention is devoted to the description of the deployable shield technology and verification.

Keywords: Mars Exploration, HDAD, Aerial Drone, DPA

Acronyms/Abbreviations

AD	Aerial Drone
CCD	Charge Coupled Device
COTS	Commercial Off The Shelf
CS	Cruise Stage
DHS	Deployable Heat Shield
DPA	Dust Particle Analyzer
EDL	Entry, Descent and Landing
ESA	European Space Agency
FS	Flexible Shield
HDAD	Hypersonic Deployable Aerodynamic Decelerator
HIAD	Hypersonic Inflatable Aerodynamic Decelerator
IRENE	Italian REentry NacellE
LEO	Low Earth Orbit
MEMS	Micro Electro-Mechanical Systems
OBDH	On-Board Data Handling
PCP	Porkchop Plot
PM	Propulsion Module
SMS	Small Mars Satellite
SOI	Sphere Of Influence
TPS	Thermal Protection System
TRL	Technology Readiness Level
UAV	Unmanned Aerial Vehicle
GCS	Ground Control Station

1. Introduction

Over the past 20 years, great effort has been put on Mars exploration, with a primary aim at understanding its surface composition and habitability potential.

Since 1976, several missions have successfully landed on Mars: Viking 1 and 2 [1], Mars Pathfinder [2], the two Mars Exploration Rovers [3], Phoenix [4] and Mars Science Laboratory [5]. All Mars landers, including those of the on-going ESA's ExoMars programme [6], are based on similar entry, descent and landing (EDL) strategies, which employ a fixed forebody for the lander. Only recent studies have focused on deployable and inflatable landing systems. Hypersonic Inflatable Aerodynamic Decelerator (HIAD) [7-9] and Hypersonic Deployable Aerodynamic Decelerator (HDAD) [10-13] technologies represent the new challenge in planetary exploration.

The aim of this contribution is to present the Small Mars Satellite (SMS) mission, whose primary goal is to test a deployable shield for Mars atmospheric entry. The shield shall provide both thermal protection and deceleration through the thin Martian atmosphere. SMS will also carry a technology payload, i.e., an aerial drone (AD) for planetary surface exploration, and a science payload, i.e., a dust particle analyzer (DPA).

Accommodating the shield in folded configuration at launch and deploying it at Mars entry, offers the advantage of increasing the mass/volume ratio at launch, thus widening the choice of the possible launchers. Moreover, the shield deployment reduces the ballistic coefficient to much lower values than previous missions of the same category, thus allowing a significantly higher deceleration in the upper and more rarefied region of the atmosphere. This brings lower thermal and dynamic loads, and the possibility of reaching subsonic conditions without the use of a supersonic parachute. These are the core characteristics of SMS. The present work illustrates in detail the choices and the methods that led to the current system's design.

In particular, Section 2 illustrates the mission and the system outline, focusing on the system configuration and the mission profile. Section 3 is devoted to the description of launch, interplanetary transfer and Mars approach. Section 4 describes the EDL phase, followed by the illustration of the design of the deployable shield. Sections 5 and 6 describe the two payloads. Conclusions are drawn in Section 7.

2. Mission and system outline

Core characteristics of SMS are the deployable shield, the low cost and the small size, features which stand out with respect to previous Mars Landers. The overall mission cost, estimated with state-of-the-art CER models for small missions, is within 120 M€, including launch and operations. Concerning the deployable shield technology, an umbrella-like mechanism will be tested to open a flexible shield providing thermal protection and aerobraking functions during Mars entry. The shield is retracted at launch and during the interplanetary cruise. This feature allows to adopt a small launcher, gives higher flexibility in the shield design and sizing, and brings advantages in the achievable ballistic coefficient at planetary entry. Indeed, the ballistic coefficient can be made sufficiently small for the deceleration through the atmosphere to subsonic Mach numbers to be achieved without a supersonic parachute, and at altitudes higher than those of previous Mars missions. This is discussed in detail in Section 4 which describes the EDL phase results and the deployable shield technology. Here, we wish to mention that a lower ballistic coefficient allows to deliver payloads at higher elevations on Mars surface, with the possibility of reaching unexplored sites, of high interest for life search [14].

As outlined in the previous section, SMS will carry on board a DPA and an AD. These are designed so to fit the limited power, mass and volume resources available on board SMS (see sections 5 and 6). Nevertheless, they can potentially improve Mars atmosphere knowledge and modeling, as well as demonstrate the viability of atmospheric flight on Mars, issues of high interest to future Mars exploration missions.

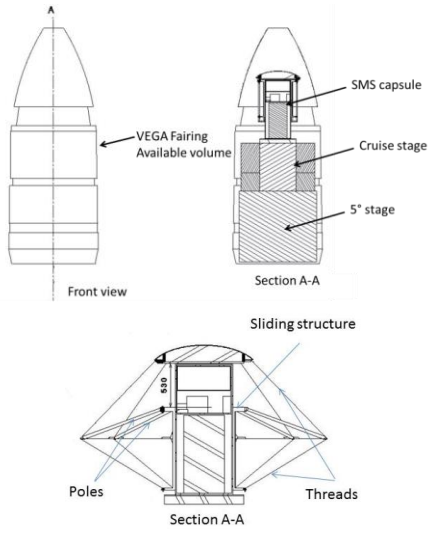

Fig. 1. Overall system configuration at launch (top) and SMS with the shield opened (bottom).

SMS will be launched to Mars by a Vega rocket on a direct hyperbolic transfer. To this end, an additional propulsion module (PM), acting as a fifth stage, shall be introduced because Vega does not perform to Earth escape. The propulsion module will separate soon after executing the injection into interplanetary trajectory. Fig. 1 illustrates the launch setup in the payload fairing of Vega: SMS (with the shield in retracted

configuration) is integrated with the Cruise Stage (CS), and the ensemble is installed on top of the fifth stage. The CS provides electric power, telecommunications, thermal control, and attitude determination and control during the interplanetary transfer, and is jettisoned shortly before Mars entry. On approaching Mars, the CS applies a targeting maneuver to achieve the required kinematics conditions at atmospheric entry (i.e., a flight path angle between -14º and -12º).

To host the payloads and carry out the mission, SMS exploits a modular architecture, which consists of two main elements: the Lander, including the payload and the avionics modules (see Fig. 2), and the deployable shield (see Fig. 1). The payload module (drone bay in the figure) hosts the AD in folded configuration, preserving its integrity during all the mission and allowing its release after landing. The avionics module contains the DPA and all the subsystems and components required to carry out the mission and perform the payload operations on Mars. A vented airbag is stowed in the hollow nose and in the upper side of the avionics bay.

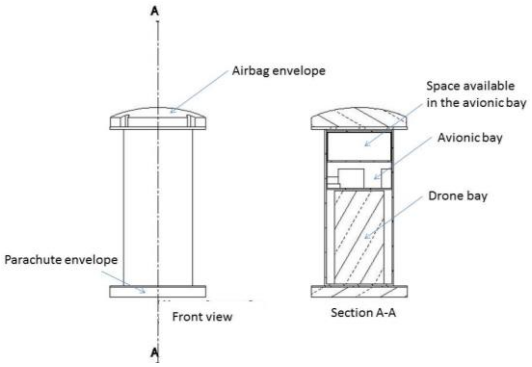

Fig. 2. SMS capsule configuration.

As outlined in Fig. 3, at Mars entry the umbrella-like mechanism unfolds the shield. Then, a subsonic parachute is opened to further reduce the ground impact speed to values compatible with a passive soft landing system (i.e., the vented airbag). The deployable shield is jettisoned soon after parachute deployment. Once on ground, the cover of the Lander unfolds (see section 6) exposing the AD. Operations on the surface of Mars should last from a few days to a few weeks.

As shown in Table 1, the wet mass is of 304.5 kg. Upon separation of the CS, the mass of the system decreases to about 200 kg. After parachute and shield ejection, the mass further decreases to 132 kg. This value is the mass at landing. About 15 kg of propellant are needed for maneuvers during cruise.

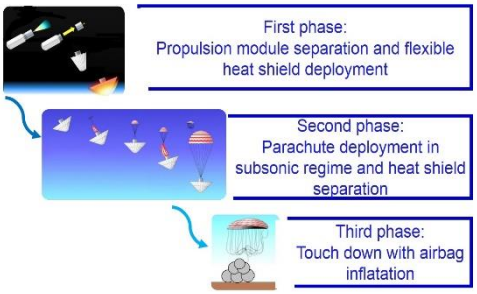

Figure 3. EDL operation sequence.

Table 1. Overall system mass budget.

Unit	Mass(kg)
Cruise Stage	74.3
Lander	110
Deployable Heat Shield	57.1
System margin (20%)	48.3
Total dry mass	289.7
Total wet mass	304.5

3. Launch, interplanetary transfer and Mars approach

SMS will follow a direct trajectory from Earth to Mars and shall enter the atmosphere of Mars from a hyperbolic orbit relative to the planet. Environmental considerations put restrictions on the choice of the landing site and on the selection of the arrival date. According to the temperature maps of Fig. 4, the southern hemisphere is characterized by the warmest temperatures, and this occurs in winter. However, the Martian atmospheric conditions are severe at this epoch because the heat transport causes strong air currents and winds which raise the dust. The dust circulation causes devils and may even result in global storms. Therefore, landing close to the equator (the mildest region on a yearly basis) before autumn is to be preferred.

Following the algorithm proposed by [15], the Earth-to-Mars trajectories have been computed by solving the two-body Sun-spacecraft Lambert's problem between positions obtained by assuming that the planets are massless bodies revolving on secularly-precessing Keplerian ellipses.

The transfer opportunities have been determined with a time resolution of one day at departure and at arrival. These opportunities are represented in the form of porkchop plots (PCPs), and their overall cost (sum of departure and arrival ΔV's) exhibits a typical pattern with a periodicity of two years approximately, resembling the synodical period of the two planets (2.14 years). Hence, three PCPs are available for the interval 2020-2024, centered in 2020, 2022 and 2024, respectively. The opportunities with the minimum cost at departure are those of the year 2024, in particular those corresponding to type II trajectories (i.e.,

trajectories with transfer angles larger than 180º) (see Fig. 5).

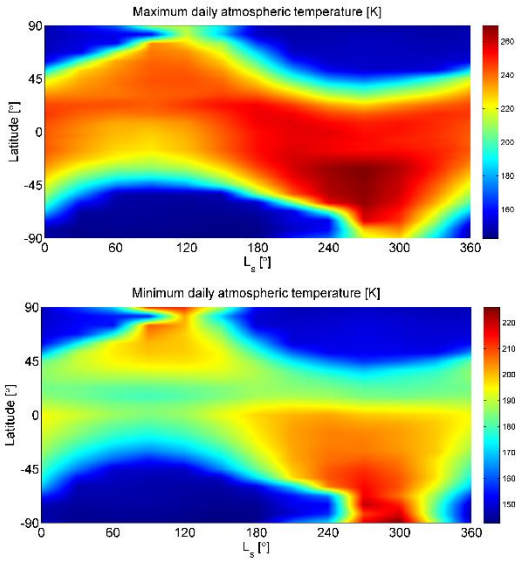

Fig. 4 - Daily average maximum (top) and minimum (bottom) atmospheric temperatures close to the ground over one Martian year and with respect to geographical latitude. The lowest minima are close to -130ºC, whereas the highest maxima are at the level of 20ºC.

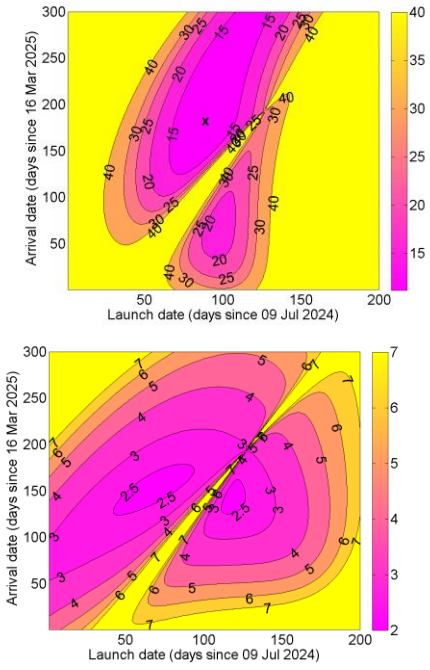

Fig. 5. Porkchop plots for the 2024 launch opportunities: colour maps of departure C_3 (km^2/s^2 top) and arrival v_∞ (km/s, bottom).

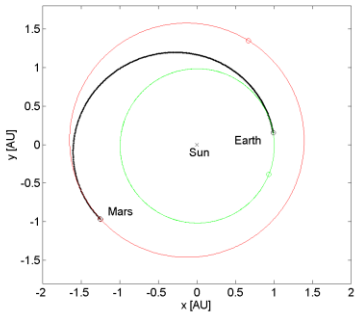

Fig. 6. Heliocentric plot of the baseline Earth-to-Mars trajectory (details in the text). The positions of Earth at arrival and Mars at departure are also indicated.

The lowest cost at departure corresponds to a 334-days trajectory leaving the Earth on 2 October 2024 and reaching Mars on 1 September 2025 (see Fig. 6). This solution has an Earth C_3 (the square of the hyperbolic excess speed v_∞) of 11.3 km^2/s^2 and a Mars v_∞ of 2.5 km/s. The arrival date is compliant with the requirement of landing before the local autumnal equinox.

The C_3 level of the trajectory sets the requirements on the wet mass of the spacecraft, in a way which depends on the performance of the launcher. Among the three European vehicles, i.e., Ariane 5, Soyuz and Vega, Vega is the cheapest and the smallest, in other words the most suitable for a small-class mission.

Unfortunately, Vega by itself launches to geocentric orbit ($C_3 < 0$) only. The performance of Vega can be enhanced to positive values of C_3 by an additional *ad hoc* stage assembled with the spacecraft and stowed in the payload fairing. In particular, according to a recent study [16], a particular bi-propellant engine (i.e., the PM) provides the performance shown in Fig. 7.

Following insertion into a 300-km LEO low-inclination orbit and separation from the launcher, the PM can inject a spacecraft of the mass indicated in the *y*-axis, given the C_3 (*x*-coordinate) and one of two options for the size of the PM's propellant tank, i.e., the short (yellow line) or the long (red line). The Lisa Pathfinder spacecraft [17] was launched to the L_1 point of the Sun-Earth system with a version of the PM: upon separation from the fourth stage of the rocket, the PM executed a series of apogee raising maneuvers until escape was achieved. The baseline launch profile that has been conceived for SMS is very similar to this. Adoption of the long propellant tank allows to launch 320 kg of wet mass, margins included. The apogee raising sequence shown in Fig. 8 is just an exercise based on the example of Lisa Pathfinder. Modifications shall be made based on communications and power requirements. However, although in a preliminary and simplified way, this apogee raising

sequence demonstrates that SMS can be injected into the right hyperbolic trajectory by means of six perigee burns of 0.4249 km/s, followed by a final burn of 0.8297 km/s of 22 minutes duration. The maneuvers performed by Lisa Pathfinder had similar magnitudes and duration.

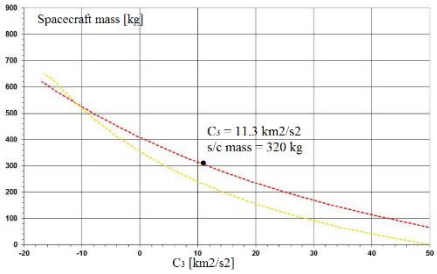

Fig. 7. Performance of Vega (launch mass, kg) with the PM endowed with either of two versions of the propellant tank (long in red, short in yellow).

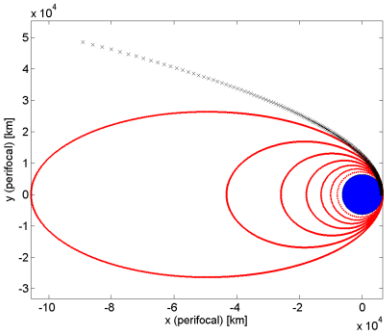

Fig. 8. A possible Earth escape sequence through seven consecutive perigee burns executed by the PM.

The selected interplanetary trajectory targets the center of Mars in a two-body Sun-spacecraft model. The gravitational influence of the planet gradually takes over as SMS approaches its destination, and, according to the patched conics model, dominates the dynamics of the spacecraft once an ideal border, i.e., the surface of the sphere of influence (SOI, 580000 km radius) has been crossed. The resulting Mars-centered hyperbola must be appropriately corrected in order to satisfy the aerodynamic requirement that the flight path angle be in the range [-14º, -12º] at an altitude of 125 km, representing the upper limit of the Martian atmosphere. The correction maneuver has been modelled as a small impulse (33 m/s) applied by the onboard propulsion system when crossing the surface of the SOI. Such impulse makes SMS enter the atmosphere at a speed of 5.5 km/s and land close to the equator, as desired.

4. The EDL phase and the deployable thermal protection system (TPS) concept layout

Here we define the SMS capsule's entry trajectory and we make a preliminary assessment of the shield design. Velocity, Mach number and pressure profiles have been computed over the entry trajectory using 3-DOF models and hypersonic Newton theory for entry trajectories evaluation.

$$\begin{cases} \dfrac{dV}{dt} = -\dfrac{\rho V^2}{2\beta} - g\sin\gamma + \\ \quad +\omega_M^2 r\cos\lambda\left(\sin\gamma\cos\lambda - \cos\gamma\sin\psi\sin\lambda\right) \\ V\dfrac{d\gamma}{dt} = \left(\dfrac{V^2}{r} - g\right)\cos\gamma + 2\omega_M\cos\lambda\cos\psi + \\ \quad +\omega_M^2 r\cos\lambda\left(\cos\gamma\cos\lambda - \sin\gamma\sin\psi\sin\lambda\right) \\ V\dfrac{d\psi}{dt} = -\dfrac{V^2}{r}\cos\gamma\cos\psi\tan\lambda + \\ \quad -2\omega_M\left(\sin\lambda - \tan\gamma\sin\psi\cos\lambda\right) - \omega_M^2 r\dfrac{\cos\psi\sin\lambda\cos\lambda}{\cos\gamma} \\ \dfrac{dH}{dt} = V\sin\gamma \\ \dfrac{d\lambda}{dt} = \dfrac{V}{r}\cos\gamma\sin\psi \\ \dfrac{d\Lambda}{dt} = \dfrac{V}{r}\dfrac{\cos\gamma\cos\psi}{\cos\lambda} \end{cases} \quad (1)$$

$$\dot{q}_0 = 1.83\cdot 10^{-4} V^3\sqrt{\frac{\rho}{R_c}} \quad (2)$$

$$p_0 = \rho V^2 \quad (3)$$

In Equation 1 t is the time, V the velocity, H the altitude, γ the flight path angle, β the ballistic coefficient, g the gravitational acceleration, r the radius of curvature of the trajectory, ψ the azimuth angle, λ the latitude, Λ the longitude and ω_M Mars angular rotation speed. Heat fluxes ($\dot{q}_0$) have been estimated along the trajectories using engineering formulations (eqn. 2) as a function of the speed V, the Mars atmospheric density ρ and the capsule nose radius R_0 [13]. Equation 3 describes the hypersonic Newton theory where p_0 is the stagnation point pressure, V the velocity and ρ the Mars atmospheric density.

Due to the low atmospheric density of Mars, all past Mars landers have employed complicated and expensive EDL strategies in order to safely touch down on the surface [14]. In these designs, the entry capsule is characterized by a fixed forebody heat shield which protects the lander in the high aerodynamic heating portion of the atmospheric entry. Then, when the capsule reaches supersonic speeds, a parachute system is deployed to reduce the speed. Once the lander has slowed down to subsonic speeds, the heat shield is jettisoned and a subsonic parachute is deployed. Different touch down methods, active and passive, using thrusters and airbags respectively, are employed.

The advantage of using a deployable umbrella-like configuration is the small attainable ballistic coefficient, which can be made lower than 20 kg/m^2, less than one third the ballistic coefficient of any previous Mars lander [18]. Compared with the EDL methods adopted by past missions, several advantages are brought by the decrease in the ballistic coefficient. First of all, the aerodynamic and aero-thermo-dynamic loads along the hypersonic entry flight path are much reduced. Besides, a single subsonic parachute may be sufficient since the capsule decelerates to subsonic speeds at higher altitudes. Finally, passive landing systems, such as airbags or crushing systems, can be used to absorb the impact energy.

A parametric analysis based on varying the ballistic coefficient and the flight path angle has been carried out in order to assess the maximum design parameters (Fig. 9). The simulations have been performed with actual values for the entry mass (200 kg) and the shield diameter (3.11 m), and assuming a drag coefficient C_d equal to 1. Special relevance has been given to the results corresponding to β = 21 kg/m^2 and FPA = -13°. The relative initial entry velocity and initial entry altitude have been set to 5.5 km/s and 125 km, respectively (see Section 3).

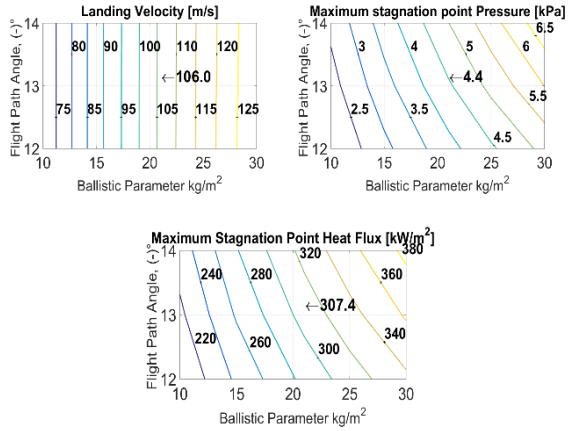

Fig. 9. Landing speed (top-left), stagnation point heat flux (top-right) and pressure (bottom) as functions of ballistic coefficient (*x*-axis) and entry FPA (*y*-axis).

Figure 10 shows a comparison between the velocity profiles of previous Mars entry trajectories [19] and the nominal SMS entry path. The lower ballistic coefficient achieved by SMS causes lower stress in terms of aerodynamic and aero-thermo-dynamic loads.

As shown in Fig. 10, one of the most important results achieved with the deployable shield technology is the possibility of reaching the subsonic regime at altitudes of approximately 15 km without sophisticated deceleration systems (such as supersonic parachutes or thrusters). Hence, the SMS technology is extremely flexible and the only low-cost system capable of landing at high altitudes (i.e., sites with elevation higher than MOLA 0).

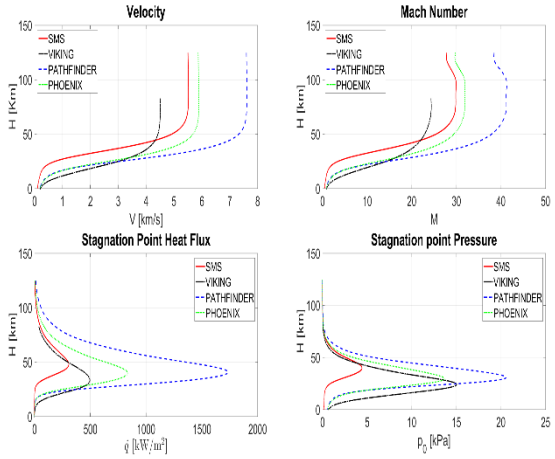

Fig. 10. Speed, Mach number, stagnation point heat flux and pressure profiles for SMS and three previous Mars landers, i.e., Mars Viking, Mars Pathfinder, Phoenix.

A parachute analysis has been carried out to assess the performance of SMS in terms of landing capability using a single subsonic parachute. In order to simulate the shield ejection in the entry trajectory after the parachute deployment, an analysis of the variation of the landing speed as a function of the Lander mass has been performed. For this analysis, four alternative values for the diameter have been considered (Fig. 11).

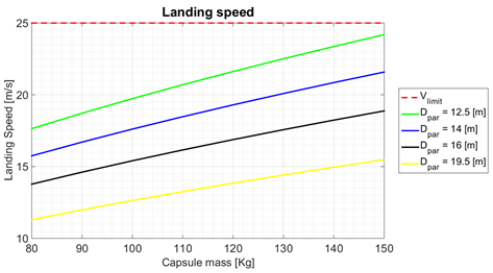

Fig. 11. Landing speed as a function of capsule mass and parachute diameter.

Finally, in order to evaluate the aerodynamic and thermal field around the entry capsule and particularly on the flexible and rigid elements of the thermal protection system, an aero-thermo-dynamic analysis on the selected capsule configuration has been executed. Depending on the flow regime, different numerical state-of-the-art codes have been applied. In continuous regime, the solution of the classical Navier-Stokes and energy equations has been obtained with the commercial code STAR-CCM+ [20]. The flow field around the capsule has been assumed laminar. Due to its chemical composition (95% carbon dioxide), the Mars atmosphere has been treated as a single-component ideal gas. The numerical simulations have

been performed with a density-based, time implicit numerical solution scheme through a control volume-based technique. The AUSM (Advanced Upstream Splitting Method) scheme has been employed for convective numerical fluxes [21, 22]. In a rarefied regime, the study of the aerodynamic characteristics has required Direct Simulation Monte Carlo (DSMC) methods [23]. In particular, two-dimensional axisymmetric analyses have allowed to estimate the distribution of the thermal and mechanical loads on the surface of the capsule, and to compare the results obtained in the EDL phase. Three-dimensional analyses have allowed to calculate the values of temperature and pressure distributions on the three-dimensional geometry of the capsule at the most severe conditions along the entry trajectory.

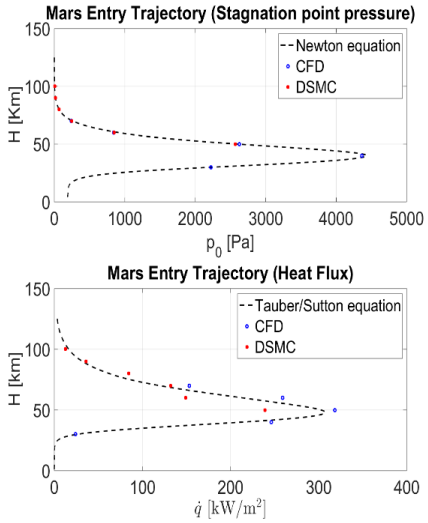

Fig. 12. CFD, DSMC and hypersonic Newtonian theory (top) and Tauber/Sutton theory (bottom).

Fig. 12 shows good agreement in terms of stagnation point pressure prediction, meaning that the Newtonian theory is a valuable tool to predict the stagnation point pressure for a blunt body in a hypersonic flow field. It is known that the correct evaluation of the stagnation point heat flux over the planetary entry trajectory is a very difficult task to accomplish. According to Fig. 12, the more rarefied the flow regime, the closer the DSMC results are to the curve predicted by the theory. On the other hand, as the altitude decreases, the CFD code results get closer to the Tauber/Sutton equation results.

Fig. 13 illustrates the pressure distribution at maximum stagnation point conditions and the temperature distribution at maximum stagnation point heat flux conditions through the capsule entry trajectory.

The main component of the TPS is a flexible shield (FS) whose deployment mechanism is essentially made up of a sliding structure, tensioning poles and threads. Figure 14 shows the shield in retracted (top) and deployed (bottom) configuration. A rigid nose cone and the associated support structure are also part of the TPS.

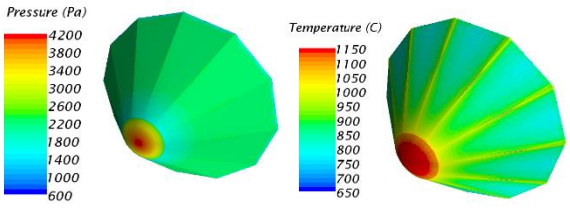

Fig. 13. Pressure distribution at maximum stagnation point pressure at 40 km (left) and temperature distribution at maximum stagnation point heat flux condition at 50 km (right).

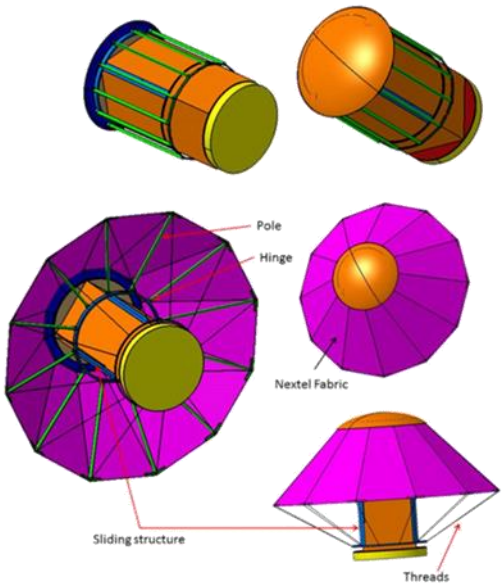

Figure 14. Shield layout in retracted (top) and deployed (bottom) configurations.

The shield is made of woven ceramic fabrics, which retain strength and flexibility with little shrinkage at temperatures lower than 1100 °C. The shield consists of two 0.38-mm layers, each composed by twelve trapezoidal patches reinforced at the edges (Fig. 15). When deployed, the shield approximates a 45° conic surface, with a maximum diameter of 3.11 m and a maximum working temperature of 1300 °C. The fabric layers are put in tension by 12 poles and are clamped at the nose cone support structure.

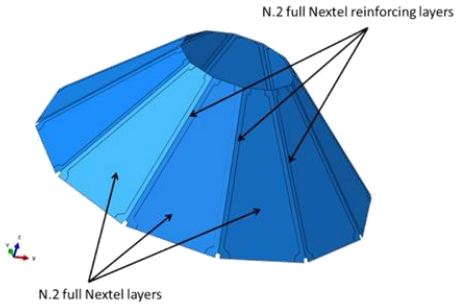

Fig. 15. Layout of the flexible shield.

In order to reduce the overall system's mass, a hollow configuration has been used for the nose cone, which offers also the possibility of accommodating the airbag. To increase the nose cone strength, a double-layer solution has been adopted in which the external layer is made of RESCOR 310M (a silica foam) with a thickness of 4 mm and a maximum working temperature of 1650 °C, and the inner layer is made of a FW12 Oxide/Oxide ceramic matrix composite with a thickness of 2 mm and a maximum working temperature of 1300 °C. Although the temperature reached at the nose during entry is equal to the maximum working temperature of FW12, the temperature at the inner layer is lower due to the 4 mm RESCOR layer. The deployment mechanism, made of titanium alloy Ti6Al-4V, is composed by a sliding structure consisting of two rings, connected by four rods, sliding along the Lander. The twelve tensioning poles (50 mm diameter, 1 mm thickness) are connected to the upper ring by means of cylindrical hinges, while the lower ring supports one end of the twelve lower threads (1.5 mm diameter). The lower and upper threads (4 mm diameter) ensure fabric stabilization in the tensioning phase before the atmospheric entry. Indeed, under pressure loads the lower threads lose tension, while the upper threads support the fabric in sustaining the loads. Two electric actuators complete the deployment system, which allow the displacement of the sliding structure during the opening phase. The shield design has been verified by using a nonlinear FE model of the flexible shield and of the main structural parts of the deployment mechanism, considering load conditions deriving from the tensioning phase and entry phase (pressure loads). A pressure value of 4.4 kPa on the nose and 3.2 kPa on the fabric have been used, as predicted by the aero-thermodynamic analysis. For the flexible shield and the deployment mechanism, both the pressure and the tensioning loads have been simulated to test the design. Fig. 16 shows the stress distribution of the Nextel fabric during entry: the stress level is lower than the allowable limit (40 MPa) except in very small areas (i.e., black areas in Fig. 16).

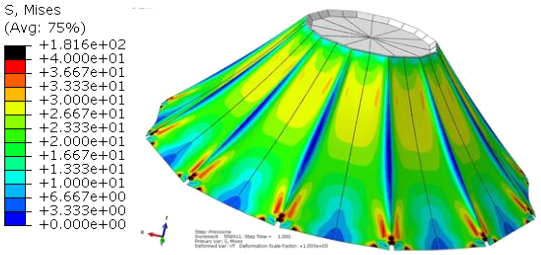

Fig. 16. Stress map on the Nextel Fabric during entry.

5. The DPA

The monitoring of airborne dust is of great interest in the study of Martian climatology because dust affects the atmospheric thermal structure, balance and dynamics by absorbing and re-emitting solar and thermal radiation.

The influence of dust is relevant, even with moderate presence of dust in the atmosphere, but during regional or global dust storms more than 80% of the incoming sunlight is absorbed by the dust causing intense atmospheric heating. Airborne dust is therefore a crucial climate component on Mars. The main dust parameters are the size distribution and abundance. Moreover, wind and windblown dust represent nowadays the most active processes having long-term effects on the Martian geology and on the morphological evolution, such as aeolian erosion, dust redistribution on the surface and weathering.

The size distribution is so far measured indirectly through remote sensing data, but these measurements exhibit poor vertical resolution, since they are related to the entire atmospheric column, and give little insight into the properties of the atmospheric layer close to the surface, where phenomena of dust lifting are present. The DPA selected for SMS will be able to perform, actually for the first time, measurements of dust concentration directly on the Martian soil. The DPA is based on an optical particle counter which processes the light scattered from the single dust particle. In this way, the instrument measures the size and estimates the abundance of each grain. As a matter of fact, according to Mie theory, the intensity of the scattered light is directly related to the grain size. The DPA is endowed with a pump to obtain a flow of gas with embedded dust flowing into the instrument, down to an area where a laser light is focused and the scattered light is collected by a mirror and finally sent to a detector. Eventually, the flow of air and dust is ejected back into the atmosphere. The light which is not scattered is captured by a light trap to avoid stray light inside the instrument. The grain radii which can be measured range from 0.2 to 10 μm, with a factor of coincidence lower than 4%. Once the particle counting and size measurements have been performed, the dust

number density can be estimated since the volume sampled by the instrument is known.

The current design of the DPA is derived from the MEDUSA instrument, selected for the ExoMars Humboldt payload which reached a TRL of 5.2 in 2009 [24]. Since the mass and power budgets are very different from those of the ExoMars mission, an optimized DPA design was needed to fulfill the more demanding requirements. The DPA has now a total mass of 600 g (including a margin of 20%) and requires about 3 W of power, instead of the 3 kg and 21 W of the MEDUSA instrument.

A DPA laboratory breadboard (Fig. 17) was developed with funds of the Italian Space Agency in 2011 and thanks to INAF financial resources afterwards. The breadboard was successfully tested demonstrating the expected performances. The estimated TRL is between 4 and 5.

Fig. 17. DPA laboratory breadboard.

The DPA will be accommodated preferably in a fixed position on the lander. The possibility of embarking the DPA on the drone was discarded because this solution is more complex and demanding, and does not ensure a significant increase in the scientific return. According to the current baseline design, the DPA will be activated after landing and shall execute at least four runs per Sol. Further activations are desired, but they depend on the availability of energy and data link resources. Longer and continuous acquisitions from the DPA can allow the detection of dust devils. Also the possibility to trigger the DPA acquisition by means of other sensors (e.g., pressure sensors) can highlight this kind of phenomena. The possibility to perform measurements with the DPA during the descent phase of SMS is also of great interest and will be studied in the next stages of the project. The DPA interfaces directly with the On-Board Data Handling (OBDH) by means of power supply and serial data interfaces.

The OBDH will activate the DPA according to a predefined mission timeline resident in the OBDH memory, and will acquire the data from the DPA after each measurement run. Scientific data can either be in the form of raw data, i.e., the complete waveform corresponding to the single event (dust grain), or can be transmitted in the form of histograms, an option which reduces the data volume.

6. The AD

Most of Mars surface exploration has been performed by means of surface rovers [25]. Rovers are able to collect data near the surface, but their exploration capability is limited by the obstacles of the terrain. To overcome these limitations, SMS carries an aerial drone.

The first idea of sending an Unmanned Aerial Vehicle (UAV) to Mars dates back to 1978 with the Mini-sniffer [27-29]. Since then, many UAV proposals have been developed including airship/balloons [30], aircraft [25, 32-34] and rotorcraft [35-38].

Among the several concepts, a two-blade coaxial rotorcraft appears the best solution in terms of deployment complexity and ability to perform multiple controlled flights while acquiring high-resolution images. In addition, this solution is compliant with the strict mass and volume requirements of the SMS mission.

The atmospheric density on Mars is about 100 times lower than on Earth, thus making the design of a Mars rotorcraft very challenging. This type of vehicle needs high blade velocity and/or radius to generate sufficient lift [25]. Furthermore, the blade design must avoid transonic regimes and Reynold numbers lower than $5 \cdot 10^4$ [35].

With this in mind, the preliminary sizing of the drone has been carried out so as to fit the space and mass available in the payload module. This has resulted in a 7-kg rotorcraft, with a rotor radius of 1.25 m. The main characteristic of the drone are summarized in Table 2.

The drone is folded inside the Lander's payload bay during launch, interplanetary flight and EDL, and is exposed by the Lander cover opening after landing.

To fulfill the high-resolution imaging goal, the drone is equipped with a COTS CCD camera, that can provide centimeter-level resolution images of the Martian surface [39]. The camera is used also as aiding sensor for navigation purposes, providing optical flow. Low-weight MEMS devices compose the drone avionics. They shall guarantee autonomous navigation and control on Mars. The drone is assumed to fly a loiter path (320 m radius, 100 m altitude, 2 km ground track) around the Lander that acts as GCS and drone landing site for battery recharging. Thus, during the flight the drone always keeps the GCS in line of sight. The multi-mission capability is ensured by four LiPo rechargeable batteries [25], which allow 7-min drone autonomous flight. The batteries are recharged in 1

SOL with the drone standing on a charging pad [40] embedded in the Lander cover (see Fig. 18).

Table 2. AD Characteristic

Parameter	Value
N. of rotors and blades (per rotor)	2
Cruise altitude (m)	100
Forward velocity (m/s)	11.5
Blade radius (m)	1.25
Main body volume (m^3)	0.15×0.15×0.15
Total power/Energy (W/Wh)	410/60

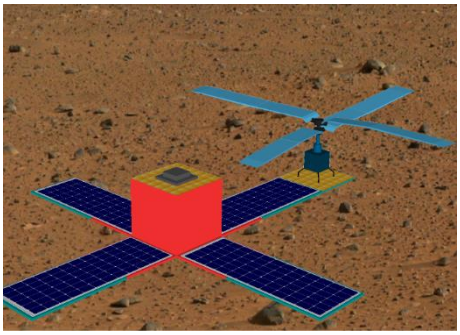

Fig. 18. Drone lading site on the unfolded lander. A charging pad is embedded in the Lander cover.

7. Conclusions

The main results of the phase 0 study of a small, low-cost system for Mars exploration have been presented. The core features of the proposed system are a flexible shield that can be deployed at Mars arrival using an umbrella-like mechanism (providing thermal protection and aerobraking functions), a small scientific payload, for atmospheric dust analysis, and a small aerial drone aiming at demonstrating atmospheric flight on Mars.

Our preliminary analyses have proven the capability of the innovative shield concept to limit thermal and pressure loads during re-entry, and to reduce the ballistic coefficient to much lower values than all previous Mars missions. In this way, the capsule decelerates to subsonic speeds in the higher atmosphere, without the aid of a supersonic parachute. In the paper, the overall system configuration and mission profile have been presented. A peculiar feature of the system is the possibility of using a small launcher, such as Vega, provided its performance is extended to Earth escape by the addition of an *ad hoc* fifth stage.

Finally, the preliminary design of the two payloads have demonstrated their compliance with such a small system, opening the way to achieving scientific and technological results of great value for future Mars exploration missions.

Acknowledgements

The study has been carried out under ESA Contract No. 4000115306/15/NL/LF/as (11/12/2015).

References

[1] Corliss, W.R., The Viking mission to Mars, Scientific and Technical Information Office, National Aeronautics and Space Administration, Washington, 1974.

[2] Golombek, M.P., The Mars Path Finder mission, Journal of Geophysical Research 102, 3953-3966, 2006.

[3] Crisp, J.A., Adler, M., Matijevic, J.R., et al., Mars Exploration Rover mission, Journal of Geophysical Research 108, 8061, 2001.

[4] Smith, P.H., and the Phoenix Science Team, The Phoenix Mission to Mars, Lunar and Planetary Science Conference 35, MackWell, S. and Stansbery, E. (Eds.), 2004.

[5] Grotzinger, J.P. Crisp, J., Vasavada, et al., Mars Science Laboratory Mission and Science Investigation, Space Science Reviews 170, 5-56, 2012.

[6] Banerdt, W.B., Smrekar, S., Lognonne, P., et al., InSight, A Discovery Mission to Explore the Interior of Mars, Lunar and Planetary Science Conference 44, 2013.

[7] Beck, R.A.S., Arnold, J.O., White, S., Fan, W., Stackpoole, M., Agrawal, P., Coughlin, S., Overview of initial development of flexible ablators for hypersonic inflatable aerodynamic decelerators, 21st AIAA Aerodynamic Decelerator Systems Technology Conference and Seminar, 2011.

[8] Sheta, E.F., Venugopalan, V., Tan, X.G., Liever, P.A., Habchi, S.D., Aero-structural assessment of an inflatable aerodynamic decelerator. NASA/CR-2010-216731, CFDRC Rept-8927/6, NF1676L-10953, 2010.

[9] Goldman, B.D., Dowell, E.H., Scott, R.C., Aeroelastic stability of a thermal protection system for inflatable aerodynamic decelerator. Journal of Spacecraft and Rockets, 52(1), 144-156, 2015.

[10] Bassano, E., Savino, R., Lo Forti, R., Ferrarotti, A., Richiello, C., Russo, G., Aurigemma, R., Punzo, F., Dell'Aversana, P., IRENE – Italian Re-Entry NacellE for Microgravity Experiments, in Proceedings of the 62nd International Astronautical Congress, CapeTown, October 3–7, IAC-11.A2.7.7, 2011.

[11] Carandente, V., Savino, R., D'Oriano, V., Fortezza, R., Deployable aerobraking earth entry systems for recoverable microgravity experiments, in Proceedings of the 65th International Astronautical Congress, Toronto, Canada, IAC-14.A2.3.8, September 2014.

[12] Carandente, V., Zuppardi, G., Savino, R., Aerothermodynamic and stability analyses of a deployable re-entry capsule. Acta Astronautica, 93, 291–303, 2014.
[13] Carandente, V., Aerthermodynamic and mission analyses of deployable aerobraking Earth re-entry systems, PhD thesis, 2014.
[14] Braun, R.D., Manning, R.M. Mars Exploration Entry, Descent and Landing Challenges, IEEEAC Paper, 2006.
[15] Standish, E.M., Keplerian elements for the approximate positions of the major planets, Solar System Dynamics, JPL/Caltech, http://ssd.jpl.nasa.gov/txt/aprx_pos_planets.pdf (last viewed 19/06/2016).
[16] Vega User's Manual Issue 4, Revision 0, Arianespace (Ed.), April 2014.
[17] CAS-ESA Call for Mission Proposals, Technical Annex, Chinese Academy of Science & ESA (Eds.), 2014.
[18] McNamara, P., The LISA Pathfinder Mission, 40th COSPAR Scientific Assembly 40, 2014.
[19] Edquist, K.T., Desai, P.N., Schoenenberger, M. Aerodynamics for the Mars Phoenix Entry Capsule, AIAA paper 2008-7219, 2008.
[20] Cd-Adapco STAR-CCM+ v10.04 User's Guide, 2015.
[21] Paterna, D., Monti, R., Savino, R., Esposito, A., Experimental and numerical investigation of Martian atmosphere entry, AIAA J. Space Rockets 39 2 227–236, 2001.
[22] Zuppardi, G., Savino, R., DSMC Aero-Thermo-Dynamic Analysis of a Deployable Capsule for Mars Entry, 2015.
[23] Bird, G.A., Molecular Gas Dynamics and Direct Simulation Monte Carlo, Clarendon Press, Oxford, 1998.
[24] Esposito, F., Colangeli, L., Della Corte, V., et al., MEDUSA: Observation of atmospheric dust and water vapor close to the surface of Mars, International Journal of Mars Science and Exploration 6, 1-12, 2011.
[25] Song, H., Underwood, C., A Mars VTOL Aerobot – Preliminary Design, Dynamics and Control, 2007 IEEE Aerospace Conference, Big Sky, MT, 3-10 March 2007.
[26] Englar, R.J., Michelson, R.C. , Navqi, M.A., Colozza, A., Planetary Exloration Using Biomimetics, An Entomopter for Flight on Mars, NIAC Fellow Conference, Lunar and Planetary Institute, Houston, Texas, 11-12 June 2002.
[27] Ulivi, P., Harland, D.M., Robotic Exploration of the Solar System, Part I: The Golden Age 1957-1982, Springer Science and Business Media, 2007.
[28] Colozza, A.J., Preliminary design of a Long-Endurance Mars Aircraft, NASA Contractor Report 185243, 1990.
[29] Minear, J., Davies, D., Malin, M., Gaffey, M., Buck, S., Strangway, D., Prinn, R., Final Report of the Ad Hoc Mars Airplane Science Working Group, Pasadena, 1978.
[30] Elfes, A., Bueno, S.S., Bergerman, M., De Paivs, E.C., Ramos, J.G., Azinheira, J.R., Robotic Airships for Exploration of Planetary Bodies with an Atmosphere: Autonomy Challenges, Autonomous Robots 14, 147-164, 2003.
[31] Gired, A.R., The Case For A Robotic Martian Airship, 12th Lighter-Than-Air Systems Technology Conference, San Francisco, 1997.
[32] Braun, R.D., Spencer, D.A., Design of the ARES Mars Airplane and Mission Architecture, Journal of Spacecraft and Rockets 43(5), 1026-1034, 2006.
[33] Noth, A., Engel, W., Siegwart, R., Recent Progress on the Martian Solar Airplane Project Sky-Saylor, 9th ESA Workshop on Advanced Space Technologies for Robotic and Automation "ASTRA", Noordwijk, 2006.
[34] Hall, D.W., Parks, R.W., On the Development of Airborne Science Platforms for Martian Exploration, Founding Convention of the Mars Society, Boulder, 1998.
[35] Datta, A., Roget, B., Griffiths, D., Pugliese, G., Sitaraman, J., Bao, J., Liu, L., Gamard, O., Design of a Martian Autonomous Rotary-Wing Vehicle, Journal of Aircraft 40(3), 461-472. 2006.
[36] Young, L.A., Vertical Lift – Not Just For Terrestrial Flight, in AHS/AIAA/RaeS/SAE International Powered Lift Conference, Arlington, VA, 2000.
[37] Landau, E., Helicopter Could Be 'Scout' for Mars Rovers, January 22 2015. http://www.jpl.nasa.gov/news/news.php?feature=4457 (last viewed 19.07.2016).
[38] Volpe, R., 2014 Robotic Activities at JPL, Jet Propulsion Laboratory, California Institute of Technology, Pasadena, CA, 2014.
[39] Point Gray – Innovation in Imaging website, https://www.ptgrey.com/ (last viewed 19.07.2016).
[40] New Skysense charging pad enables drones to dock recharge and fly again, 4 November 2014, http://www.skysense.co/blog/2014/11/charging-pad-drones-dock (last viewed, 19.07.2016).